

# Diffuse flux of ultra-high energy photons from cosmic-ray interactions in the disk of the Galaxy and implications for the search for decaying super-heavy dark matter

Corinne Bérat<sup>1</sup>, Carla Bleve<sup>1</sup>, Olivier Deligny<sup>2</sup>, Pierpaolo Savina<sup>2,3</sup>, François Montanet<sup>1</sup>, and Zoé Torrès<sup>1,\*</sup>

<sup>1</sup>Laboratoire de Physique Subatomique et de Cosmologie, CNRS/IN2P3, Université Grenoble Alpes, Grenoble, France

<sup>2</sup>Laboratoire de Physique des 2 Infinis Irène Joliot-Curie, CNRS/IN2P3, Université Paris-Saclay, Orsay, France

<sup>3</sup>University of Wisconsin-Madison, Department of Physics and WIPAC, Madison, WI, U.S.A

**Abstract.** When propagating to Earth, UHECRs can interact with the gas in our Milky Way and produce secondary particles including photons. This can impact the search for UHE photons as we face a diffuse flux of UHE photons resulting from their propagation. This flux, together with the photon flux expected from the GZK interactions, participates in the diffuse photon flux which is limiting the detection of UHE-gamma sources. We present an estimate of the diffuse flux resulting from the interactions of UHECRs in our galaxy above  $10^{17}$  eV, using results from the Pierre Auger Collaboration concerning the flux and its composition, and two different interstellar gas density models. We also discuss the impact of the evaluated diffuse flux of UHE photons on SHDM searches, as the former can be considered as a floor below which other signals would be overwhelmed. Similarly, the neutrino flux produced during the same process can be evaluated, by accounting for the neutrino mixing.

## 1 Introduction

On their way to Earth, UHECRs may interact with the interstellar gas in our galaxy. Above  $10^{17}$  eV, the cosmic ray flux composition consists of protons and heavier nuclei. Hence, the cosmic rays interact with the interstellar gas through nucleon-nucleon collisions, whereas at lower energies other interactions can also take place, such as Bremsstrahlung and inverse-Compton. Following these interactions, secondary particles such as UHE photons are produced. This additional flux of UHE photons can be problematic in the search for UHE photons. Indeed, these photons do not originate from the vicinity of potential astrophysical sources of UHECRs, but are the result of their propagation. By combining the knowledge of this flux, with that of GZK photons, one could estimate the diffuse flux limiting the detection of UHE photons coming from actual sources.

In this contribution, we give an estimate of the flux of UHE photons arising from the irradiation of the interstellar gas above  $10^{17}$  eV. The full study has been published in [1]. These photons essentially propagate through the galaxy without interacting, as their mean free path is higher than the galactic diameter in this energy range, as showed in Fig. 1 [2]. Therefore, the estimation of the diffuse flux per steradian of UHE photons with an energy  $E_\gamma$ ,  $\phi_\gamma(E_\gamma, \mathbf{n})$  can be simply done by integrating the emission rate at position  $\mathbf{n}$ ,  $q_\gamma(E_\gamma, \mathbf{n})$ , per unit of volume and energy along the line of sight, as follows :

\*e-mail: torres@lpsc.in2p3.fr

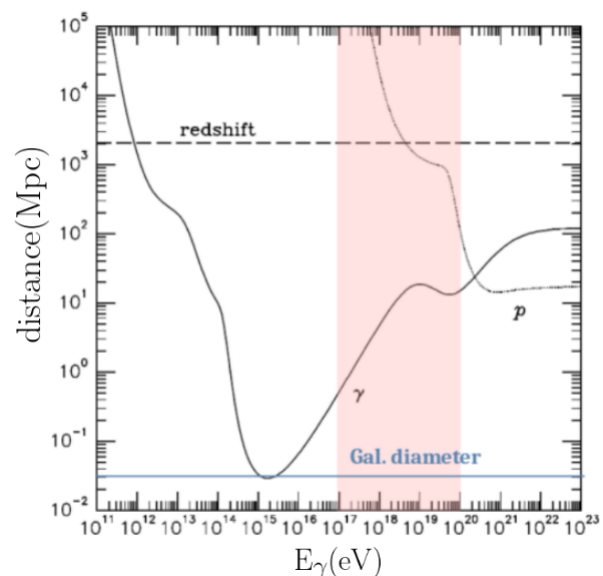


**Figure 1.** The attenuation distance of photons as function of the photon's energy. The energy range considered is showed by the pink area. The galactic diameter is reported by the blue line. Figure taken from [2].

$$\phi_\gamma(E_\gamma, \mathbf{n}) = \frac{1}{4\pi} \int_0^\infty ds q_\gamma(E_\gamma, s\mathbf{n} + \mathbf{x}_\odot) \quad (1)$$

Here,  $\mathbf{x}_\odot$  is the position of the solar system in the galaxy, and  $\mathbf{n} \equiv \mathbf{n}(l, b)$  is a unit vector on the sphere

pointing to the longitude  $l$  and latitude  $b$  in galactic coordinates. It is important to note that above  $10^{17}$  eV, the observation of UHECRs shows a high degree of isotropy [3], which leads to a equally isotropic irradiation of the interstellar gas and therefore an isotropic emission of UHE photons, hence the  $\frac{1}{4\pi}$  factor in Eq. 1.

To compute the emission rate  $q_\gamma(E_\gamma, \mathbf{x})$ , corresponding to the number of photons of energy  $E_\gamma$  produced by UHECRs with energy above  $E_0 = 10^{17}$  eV at position  $\mathbf{x}$  in the galaxy, we consider :

- The inelastic cross section of the interaction gas-UHECR :  $\sigma(E_{CR})$ .
- The UHECR flux  $\Phi_{CR}(E_{CR})$  which can be decomposed in four nuclei groups: H, He, CNO and Fe. This is done so that we can use the data from the Pierre Auger Collaboration in section 2.
- The mean number of UHE photons of energy  $E_\gamma$  produced during the interaction of an UHECR of energy  $E_{CR}$  with the interstellar gas :  $\frac{dN}{dE_\gamma}(E_{CR}, E_\gamma)$ .
- The Milky Way interstellar gas density in nuclei per  $\text{cm}^3$  in at position  $\mathbf{x}$  :  $\rho(\mathbf{x})$ .

$$q_\gamma(E_\gamma, \mathbf{x}) = 4\pi \sum_{i,j} \rho_j(\mathbf{x}) \int_{E_0}^{\infty} dE_{CR} \Phi_{CR,i}(E_{CR}) \sigma_{i,j}(E_{CR}) \frac{dN_{i,j}}{dE_\gamma}(E_{CR}, E_\gamma) \quad (2)$$

In Eq. 2, the summation over  $j$  corresponds to the different interstellar gas elements : molecular and atomic hydrogen, and helium. The one over  $i$  accounts for the four groups of UHECRs nuclei defined above.

## 2 Cosmic Ray Flux

Above  $10^{17}$  eV, the energy spectrum of cosmic rays and its mass composition are obtained via the indirect measurements of extensive air showers. With measurements of the slant depth corresponding to the maximum of the shower development, a parameter strongly correlated to the mass of the primary cosmic ray, the composition is determined on a statistical basis.

To obtain the cosmic ray flux for a defined group of primaries  $\Phi_{CR,i}(E_{CR})$ , we combine the all-particle spectrum of UHECRs,  $\Phi_{CR}(E_{CR})$ , with the energy-dependent abundances of the primaries  $f_i$ , giving :  $\Phi_{CR}(E_{CR}) = \sum_i f_i \Phi_{CR,i}(E_{CR})$ .

As for the spectrum, we used the one measured at the Pierre Auger Observatory [4] using the surface detector. This choice was made because the observatory owns the largest cumulated exposure. It also uses a single type of detector avoiding the combination of measurements and therefore the addition of systematics to the study. Uncertainties on the spectrum must be

propagated when calculating the diffuse flux. Finally, the primary energy is known calorimetrically as it is measured by the fluorescence telescopes of the observatory, allowing no assumption on the mass of the particle.

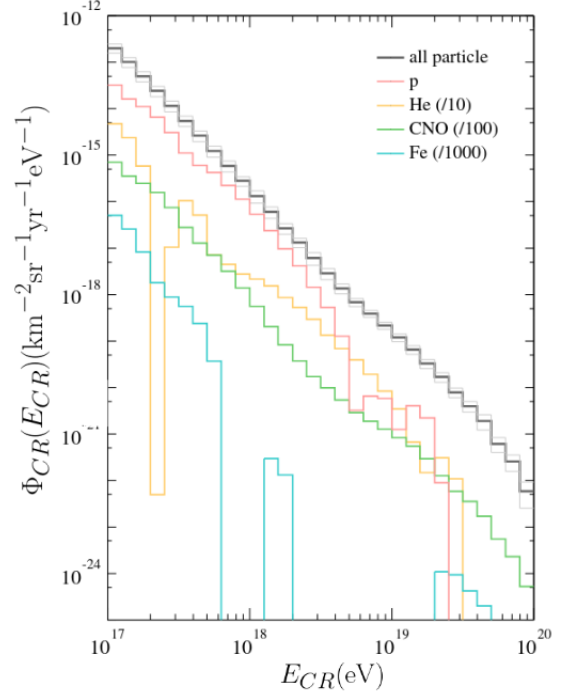


**Figure 2.** The all particle spectrum from [4] (black) with the contributions of H (red), He (orange), CNO (green) and Fe (blue).

Concerning the fraction of the four primary groups, they are also obtained from measurements carried at the Pierre Auger Observatory. The determination of the primary composition is performed by comparing the measured maximum of development of the shower, with expectations according to high energy hadronic interaction models for the four types of nuclei introduced before. We use the results from [5], where the fractions of the different primary groups are reported as a function of the cosmic ray energy, namely EPOS-LHC [6], Sibyll2.3 [7] and QJSJetII-04 [8].

Fig. 2 shows the combination of the all particle spectrum with the abundances of the nuclei types. Except for Hydrogen, the species have been re-scaled for clarity issues (see legend). The systematic uncertainties arising from both the all-particle spectrum of UHECRs and the fractions of mass groups inferred from the three different hadronic interaction models, will be propagated when calculating the estimate of the diffuse flux. As a cross-check, we took the fractions from the Global Spline Fit (GSF) [9], a data-driven fit using different ground based experiments. We regained similar results for the estimate of the flux in section 5.

### 3 Interstellar Gas Density

The interstellar gas in the Milky way is mostly composed of Hydrogen (90%) and Helium (10%), distributed essentially in the disk. Hydrogen, contributing to most of the interstellar gas mass, can be found in three different forms depending on its temperature : atomic  $H_I$ , molecular  $H_{II}$  and ionised. On the other hand, Helium stays neutral as its first ionisation potential is higher. The case of ionised hydrogen will not be considered in this work as its contribution is smaller.

The distribution of the  $H_I$  component, representing about two thirds of the Hydrogen mass, is rather constant in the distance range [4-10 pc] from the galactic centre and falls at larger distances. The density decreases exponentially in the perpendicular direction to the galactic plane with a scale length depending on the gas temperature. This distribution is known following observations via the 21-cm radio hyperfine line, whether by absorption or emission. In the case of  $H_{II}$ , the observation is not direct. Indeed, a homo-nuclear diatomic molecule like  $H_{II}$  does not possess a permanent electric dipole moment, and therefore has no simple rotational transition. Thus, the column density of  $H_{II}$  is inferred through the observations of carbon dioxide (CO) emission lines. Molecules of CO, the second most abundant molecule in the interstellar medium after  $H_{II}$ , are excited by their collisions with  $H_{II}$  molecules, resulting in a correlation between the integrated intensity of CO lines and the column density of molecular hydrogen. Finally, the distribution of Helium is not really known, being only observable in a specific ionised state. Therefore, it is assumed that it follows the hydrogen distribution but with a factor 10%.

We use two recent models of gas distribution relying on data, and compute the diffuse flux for both. The differences between the results will contribute to the systematics of  $\phi_\gamma(E_\gamma, n)$ .

The first model considered, labelled as model A in the following and developed by [10], captures the large-scale characteristics of the distribution without attempting to describe finer details. Thus, this distribution is axially and up-down symmetric neglecting features like the spiral arms and the disk wrap of our galaxy. In this model, the gas is concentrated along the galactic plane with a thickness increasing with the distance to the galactic centre  $r$ . The column density averaged on the galactic longitude  $l$ , is reported in Fig. 3 by the grey lines for atomic (plain) and molecular (dashed) Hydrogen, as function of the galactic latitude  $b$ .

The second model of interstellar gas distribution, referred as model B hereafter, was developed by [11]. This is a more detailed description with the modelisation of the spiral arms as well as the wrapping of the disk, which is useful for studying cosmic ray propagation and traces the structure of the Galaxy. The full parametrization of the model can be found in [11]. Moreover, as for model

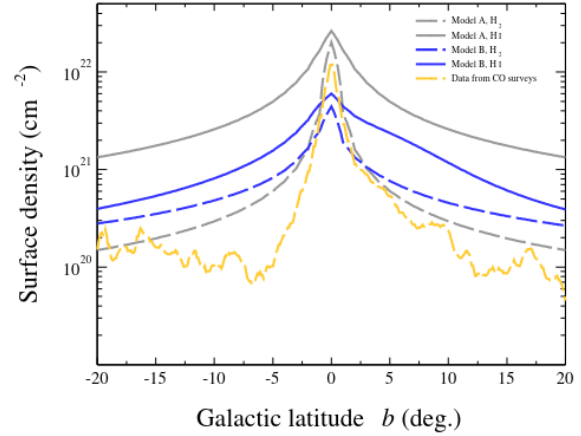


**Figure 3.** The surface density average over Galactic longitude as a function of Galactic latitude for atomic and molecular hydrogen, for model A [10] in grey and in blue for model B [11]. The surface density of molecular Hydrogen as obtained from the composite survey of [12] is shown by the orange line.

A, the surface density averaged on the galactic longitude  $l$  is also shown in Fig. 3 by the blue lines.

When summing the surface density of  $H_I$  and  $H_{II}$ , we observe a difference of the order of a few units of  $10^{22} \text{cm}^{-2}$  in the surface density averaged over the galactic longitude. These differences will be contributing in the systematics when calculating the photon flux in section 5.

### 4 Production of UHE Photons

Neutral pions  $\pi^0$  are among the secondary particles produced following the interaction of the UHECRs with the gas. They play a key role as their most probable decay mode is two photons:

$$\pi^0 \rightarrow 2\gamma$$

The production of secondaries such as  $K, \rho, \eta$ , decaying into  $\pi^0$  also occurs during the interaction, resulting in an additional flux of photons.

To obtain the inelastic cross sections  $\sigma_{i,j}(E_{CR})$  along with the energy spectra of UHE photons  $\frac{dN_{i,j}}{dE_\gamma}(E_{CR}, E_\gamma)$ , we use Cosmic Ray Monte Carlo (CRMC) [13]. This package gives access to several cosmic ray event generators that model the production of secondary particles following a hadronic interaction. It also allows the follow-up of the decays of the secondary particles that are likely to produce photons. In this work, we chose the hadronic interaction model EPOS-LHC [6].

Using CRMC, we simulate 100,000 collisions for each couple  $(i, j)$  of UHECR and gas element, for different energies of UHECR ranging from  $10^{17}$  to  $10^{20}$  eV (in steps of  $\Delta \log_{10}(E_{CR}) = 0.5$ ). The spectra of the photon energies are then produced for each cosmic ray energy,

with a bin width of  $\Delta \log_{10}(E_\gamma) = 0.05$ .

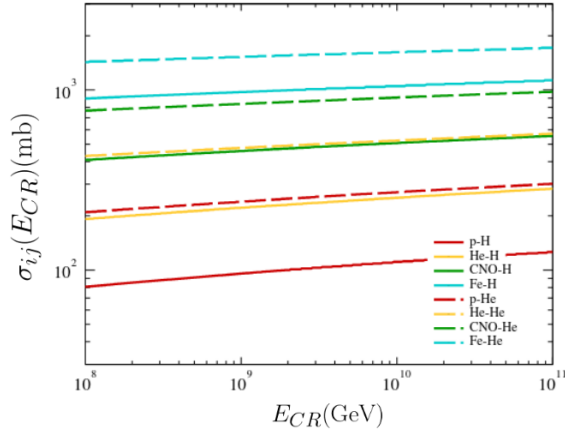


**Figure 4.** The inelastic cross sections  $\sigma_{i,j}(E_{CR})$  obtained with CRMC, as function of the cosmic ray energy, for each couple (i,j) of cosmic ray and gas element.

The inelastic cross sections given by CRMC are reported in Fig. 4 as function of the cosmic ray energies. They are of the order of a couple of hundreds of mb, up to thousands for those involving heavier elements. The photon yields  $\frac{dN_{i,j}}{dE_\gamma}(E_{CR}, E_\gamma)$  are shown in Fig. 5 for three different cosmic ray energies ( $10^{18}$ ,  $10^{19}$  and  $10^{20}$  eV). One can note that, as expected, for a fixed photon energy, the photon yields increase with the cosmic ray energy. On the other hand, for a fixed cosmic ray energy, the yields seem to depend on the mass. Indeed, during the interaction, only a single nucleon intervenes. The energy per nucleon being divided by the atomic number A, the number of photons produced is bigger for higher cosmic ray energies and lighter masses.

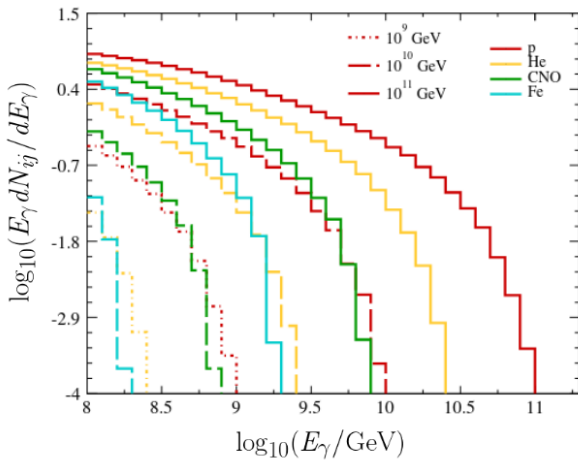


**Figure 5.** The photon yields  $\frac{dN_{i,j}}{dE_\gamma}(E_{CR}, E_\gamma)$  obtained with CRMC, for different cosmic ray energies and UHECR masses.

## 5 Diffuse Flux of UHE Photons

By combining the various ingredients introduced in the previous sections in Eq. 2, then Eq. 1, we obtain the diffuse flux of UHE photons. The results for both models of interstellar gas distribution are reported in Fig. 6 for model A and in Fig. 7 for model B. As expected, the flux is concentrated along the galactic plane, reaching  $\approx 8.7 \cdot 10^{-2} \text{ km}^{-2} \text{ yr}^{-1} \text{ sr}^{-1}$  when averaged over  $|b| < 5^\circ$  in case of model A ( $\approx 3.2 \cdot 10^{-2} \text{ km}^{-2} \text{ yr}^{-1} \text{ sr}^{-1}$  for model B).

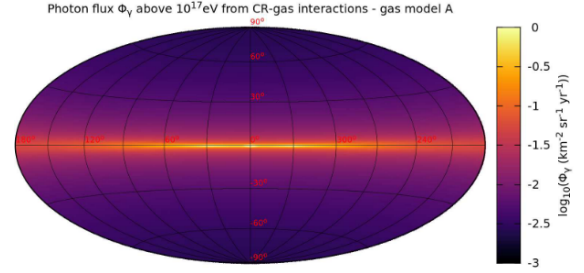


**Figure 6.** The diffuse flux UHE photons with  $E_\gamma > 10^{17}$  eV in Galactic coordinates, for model A.

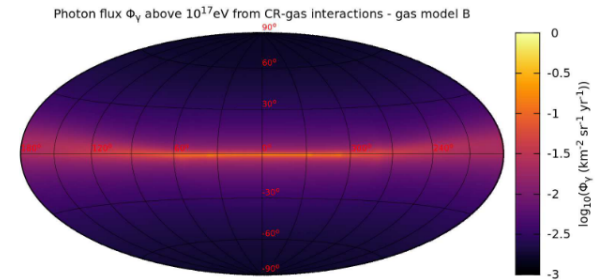


**Figure 7.** The diffuse flux UHE photons with  $E_\gamma > 10^{17}$  eV in Galactic coordinates, for model B.

The energy spectrum has a similar slope as the UHECR spectrum, but is shifted a decade down in energy. When averaged over a  $5^\circ$  band around the galactic plane, we find that its value is about  $10^{-5}$  that of the UHECRs when considering energy thresholds between  $10^{17}$  to  $10^{18}$  eV. For higher thresholds however, the spectrum of UHE photons becomes steeper, and this ratio decreases to  $10^{-6}$  for thresholds above  $10^{19}$  eV, before dropping sharply at highest energies.

$$\psi_\gamma(l) = \frac{1}{2 \cdot \sin(5^\circ)} \int dE_\gamma \int d\sin(b) \int d\mathbf{n}' f_{\theta_0}(\mathbf{n}, \mathbf{n}') \phi_\gamma(E_\gamma, \mathbf{n}) \quad (3)$$

The calculated photon fluxes can be compared to searches for UHE photons fluxes above  $10^{17}$  eV. The directional

limits reported in [14], for energies ranging from  $10^{17.3}$  to  $10^{18.5}$  eV, come from a search for point-like sources in the exposed sky of the Pierre Auger Observatory (zenith angles below  $60^\circ$ ). These limits averaged over a  $5^\circ$  band around the galactic plane are reported as the red line in Fig. 8, as function of the galactic longitude  $l$ . To compare our work to these results, we convert our directional fluxes into a collection of point-like sources detected through the point-spread function of the Pierre Auger Observatory  $f_{\theta_0}$ . This is equivalent to applying a Gaussian filter on the sphere with an angular scale of  $\theta_0 = 1^\circ$ , as seen in Eq. 3. The integration range of the photon energy is the one mentioned before, and  $b$  ranges from  $-5$  to  $5^\circ$ . The limits in this work were computed with the EPOS-LHC hadronic interaction model. However, the choice of the hadronic interaction model when creating the photons energy spectra with CRMC only intervenes at the second order in the computation, thus it does not impact the results. They are reported for model A and B by the grey and blue bands respectively, and are about 3 orders of magnitude below the limits reported in [14]. The bands depict the systematics coming both from those in the UHECRs spectrum and in the different hadronic interaction models used in the determination of the mass composition. The propagation of uncertainties can be found in [1]. One can conclude easily that these limits cannot be reached with current observation capabilities. Although these limits could be improved by a factor 2 or 3 by collecting more data at the Pierre Auger Observatory, the conclusion would be the same. Moreover, the limits reported here are for a  $E_\gamma^{-2}$  photon spectrum, the difference would be higher for steeper spectra.

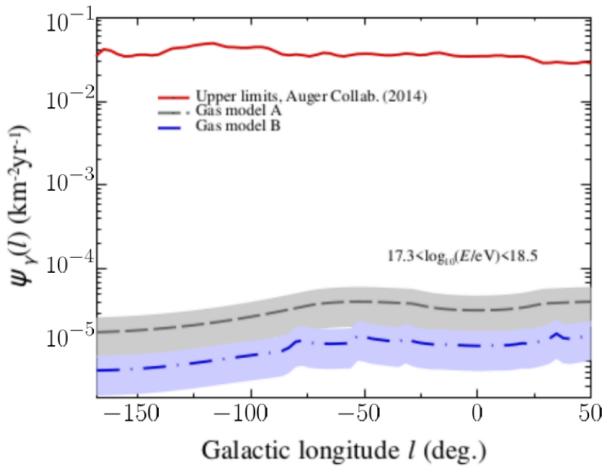


**Figure 8.** The directional photon fluxes averaged over an  $5^\circ$ -band along the galactic plane, when converting the fluxes into a collection of point-like sources detected through the point-spread function of the Auger Observatory. The energy range considered ranges from  $10^{17.3}$  to  $10^{18.5}$  eV. Dashed: gas model A. Dotted-dashed: gas model B. Continuous red line: upper limits at 95% confidence level obtained at the Pierre Auger Observatory [14].

The UHE photons fluxes obtained can also be compared to other searches for a diffuse flux above  $10^{17}$  eV,

performed by several experiments like EAS-MSU [15], KASCADE-Grande [16], Telescope Array [17], and the Pierre Auger Collaboration [18]. The upper limits for each of them are reported of Fig. 9 by an orange dot, a black dot, a pink triangle and a blue square respectively, while our results correspond to the blue and grey bands. One must note that, to compare to upper limits on the diffuse fluxes illuminating the whole field of view of the observatory considered, it is needed to calibrate the expected fluxes on the whole sphere, as showed in Eq. 4. The limits obtained by the different observatories appear to be between 2.5 to 3 orders of magnitude above our expectations for energy thresholds between  $10^{17}$  and  $10^{18}$  eV, and even higher for larger thresholds.

$$\Phi_\gamma(E_\gamma) = \frac{1}{4\pi} \int_{E_\gamma}^{\infty} dE'_\gamma \int_{4\pi} d\mathbf{n} \phi_\gamma(E'_\gamma, \mathbf{n}) \quad (4)$$

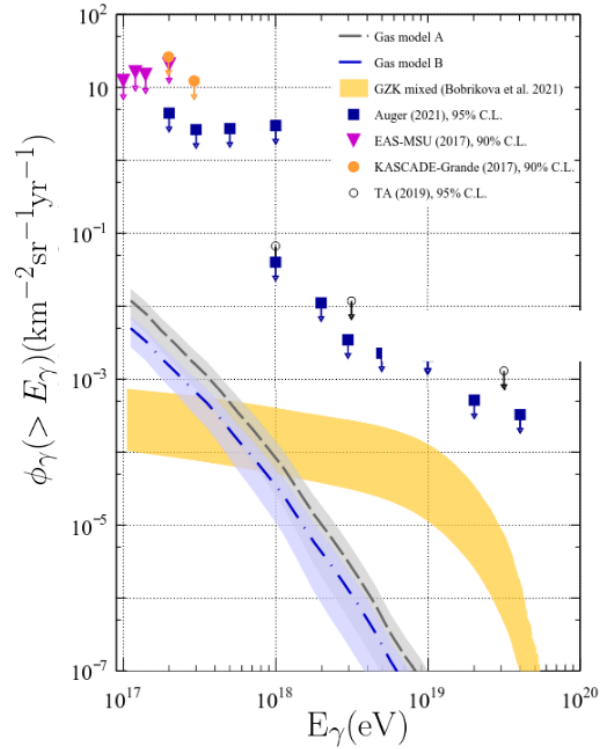


**Figure 9.** Upper limits on diffuse photon fluxes reported by [15] (pink triangles, EAS-MSU), [16](filled orange circles, KASCADE-Grande), [17](open circles, Telescope Array), and [18](dark blue squares, Auger). Expected fluxes from UHECRs interactions with the gas distribution in the Galaxy are shown as the grey dashed line (model A) and grey dashed-dotted line (model B), as well as from UHECRs interactions with background photon fields (GZK mixed) estimated by [19].

In Fig. 9, the orange band represents the expected GZK photon flux reported in [19], a cosmogenic photon flux arising from the interaction of UHECRs with the photon fields present the universe. This flux depends on the nature of the UHECR and it is reported here for a

mixed composition fitting the Pierre Auger Observatory data, namely the measured energy spectrum and mass composition. The systematic uncertainties arising from these measurements lead to the orange band.

For energy thresholds between  $10^{17}$  and  $10^{18}$  eV, we expect the cosmogenic flux originating from the interactions of UHECRs with the interstellar gas to be the dominant one, while the GZK takes over for higher thresholds.

## 6 Implication on SHDM Searches

The region between  $10^{17}$  to  $10^{18}$  eV, where the flux computed in this work is dominant, is of interest. Indeed, it can be seen as a floor that could prevent probing sources, in particular in the galactic disk, or indications on the presence of super-heavy dark matter (SHDM) produced in the early universe and decaying today generating a photon flux  $\phi_\gamma^{DM}$  in the direction of the galactic centre. In the field of SHDM searches, a photon flux in this peculiar direction has important implications. Depending on the mass of the super heavy particle  $M_X$ , the photon flux can be translated into a ceiling for the life-time  $\tau_X$  of this particle.

The production of UHE photons following the decay of SHDM particles can occur if these particles have a long enough life-time. This is possible when they are protected from decays in the perturbative domain, but disintegrate by what is called instanton non-perturbative effects [20]. This mechanism provides metastable particles of life-time  $\tau_X$  which can produce secondary particles such as photons. The expected photon flux from these decays can be obtained by integrating the position-dependent emission rate per unit volume and energy along the direction  $\mathbf{n}$  as in [21]:

$$\phi_\gamma^{DM}(E_\gamma, \mathbf{n}) = \frac{1}{4\pi M_X \tau_X} \frac{dN}{dE_\gamma} \int_0^\infty ds \rho_{DM}(\mathbf{x} + s\mathbf{n}) \quad (5)$$

In Eq. 5,  $\rho_{DM}$  is the energy-density profile of dark matter in the galaxy, and  $\frac{dN}{dE_\gamma}$  represents the energy spectrum of UHE photons produced in the decay which depends on the hadronization process. In this work we considered the Navarro-Frenk-White profile found in [22], normalized so that  $\rho(\odot) = 0.3 \text{ GeV.cm}^{-3}$ . In [23], it is shown that the spectra of the final state particles, varies as  $E^{-1.9}$ , and we used this energy dependence in the following.

It is possible to infer constraints in the  $(M_X, \tau_X)$  plane from the limits on UHE photon fluxes by requiring that  $\phi_\gamma^{DM}(E)$ , the flux presented in Eq. 5 averaged over all directions  $\mathbf{n}$ , is smaller than the limits. Indeed, for an upper limit at a certain energy threshold, one can scan the value of  $M_X$  in order to obtain a lower limit on the life-time  $\tau_X$ . By repeating the procedure on all energy thresholds, we obtained a collection of excluded regions

of  $(M_X, \tau_X)$  whose sum is reported as the red area on Fig. 10.

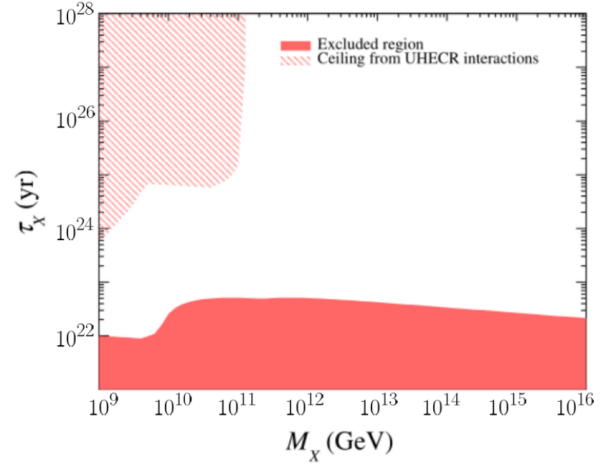


**Figure 10.** Allowed region of mass and life-time of SHDM particles decaying into standard-model ones. The filled red region is excluded from the upper limits in UHE photon fluxes. The hatched one corresponds to the ceiling region discussed in section 5

Finally, by scanning  $M_X$  we can also determine the corresponding  $\tau_X$  for which  $\phi_\gamma^{DM}(E_\gamma) < \phi_\gamma(E_\gamma)$ , meaning that the flux originating from dark matter is overwhelmed by the cosmogenic flux. This results in a ceiling region showed in Fig. 10 as the pink hatched area. The ceiling affects masses up to  $10^{11}$  GeV, which corresponds to the cut-off in the cosmogenic photon fluxes. While masses below  $10^{10}$  GeV are constrained by the photon flux discussed in this work, for masses above this threshold the GZK expected photon flux from [19] takes over. In the end, a large region of the plane remains unaffected by the ceiling.

## 7 Conclusion and Outlooks

The expected flux of UHE photons above  $10^{17}$  produced by the interactions of UHECRs with the interstellar gas amounts to  $1.1 \times 10^{-2} \text{ /km}^2\text{/yr/sr}$  (a few degrees around the galactic plane). It is the dominant cosmogenic one in the energy thresholds ranging from  $10^{17}$  to about  $10^{18}$  eV. Although its detection remains out of reach for current observatories, it is relevant for searches on SHDM in the direction of the galactic centre, as it sets a floor below which other signals would be overwhelmed. Indeed, the results set a floor for a ceiling region for the life-time of SHDM particles that seems to affect masses up to  $10^{11}$  GeV.

A similar interesting study is ongoing at a lower threshold in energy of  $10^{15}$  eV, with other neutral messengers such as neutrinos produced by charged pions decays. In this case, the abundances of nuclei are taken from the GSF [9] mentioned in section 2. Moreover, when decreasing the energy threshold, one has to account for the anisotropy of UHECRs sources and add the contribution

of galactic sources of cosmic rays. As for now, the flux has been computed with the assumption of the isotropy of UHECRs and appears to be below current upper limits on neutrino fluxes.

## References

- [1] C. Bérat, C. Bleve, O. Deligny, F. Montanet, P. Savina, Z. Torrès, *The Astrophysical Journal* **929**, 55 (2022)
- [2] Sangjin Lee, *Physical Review D* **58**, 043004 (1998)
- [3] Alexander Aab et al., *The Astrophysical Journal* **891**, 142 (2020)
- [4] Alexander Aab et al., *The European Physical Journal C* **81**, 996 (2021)
- [5] J. Bellido, *PoS ICRC2017*, 506 (2018)
- [6] T. Pierog, I. Karpenko, J.M. Katzy, E. Yatsenko, K. Werner, *Physical Review C* **92** 034906 (2015)
- [7] F. Riehn, H.P. Dembinski, R. Engel, A. Fedynitch, T. Gaisser, T. Stanev, *PoS ICRC2017*, 301 (2017)
- [8] S. Ostapchenko, *EPJ Web of Conferences* (EDP Sciences,2013) 02001
- [9] H. Dembinski, R. Engel, A. Fedynitch, T. Gaisser, F. Riehn, T. Stanev, *PoS ICRC 2017*, 533 (2017)
- [10] P. Lipari, S. Vernetto, *Physical Review D* **98** 043003 (2018)
- [11] J. Gudlaugur, T.A. Porter, I.V. Moskalenko, *The Astrophysical Journal* **856**, 45 (2018)
- [12] T.M. Dame, D. Hartmann, P. Thaddeus, *The Astrophysical Journal* **547**, 792 (2001)
- [13] R. Ulrich, T. Pierog, C. Baus, *Cosmic Ray Monte Carlo Package, CRMC* (2021) source
- [14] A. Aab et al., *The Astrophysical Journal Letters* **789**, 160 (2014)
- [15] Y.A. Fomin, N.N. Kalmykov, I.S. Karpikov, G.V. Kulikov, M.Y. Kuznetsov, G.I. Rubtsov, V.P. Sulakov, S.V. Troitsky, *Physical Review D* **95**, 123011 (2017)
- [16] W.D. Apel et al., *The Astrophysical Journal* **848**, 1 (2017)
- [17] R.U. Abbasi et al., *Astroparticle Physics* **110**, 8–14 (2019)
- [18] P. Savina, *PoS ICRC2021*, 373 (2021)
- [19] A. Bobrikova, M. Niechciol, M. Risse, P. Ruehl, *PoS ICRC2021*, 449 (2021)
- [20] V.A. Kuzmin, V.A. Rubakov, *Physics of Atomic Nuclei* **61**, 1028 (1998)
- [21] R. Aloisio, V. Berezhinsky, M. Kachelriess, *Physical Review D* **74**, 023516 (2006)
- [22] J.F. Navarro, C.S. Frenk, S.D.M. White, *The Astrophysical Journal* **462**, 563 (1996)
- [23] R. Aloisio, V. Berezhinsky, M. Kachelriess, *Nuclear Physics B Proceedings Supplements* **136**, 319 (2004)